eprints@whiterose.ac.uk
https://eprints.whiterose.ac.uk/

THE PLANE WAVES METHOD FOR NUMERICAL BOUNDARY IDENTIFICATION

A. KARAGEORGHIS, D. LESNIC, AND L. MARIN

ABSTRACT. We study the numerical identification of an unknown portion of the boundary on which either the Dirichlet or the Neumann condition is provided from the knowledge of Cauchy data on the remaining, accessible and known part of the boundary of a two-dimensional domain, for problems governed by Helmholtz-type equations. This inverse geometric problem is solved using the plane waves method (PWM) in conjunction with the Tikhonov regularization method. The value for the regularization parameter is chosen according to Hansen's L-curve criterion. The stability, convergence, accuracy and efficiency of the proposed method are investigated by considering several examples.

1. INTRODUCTION

The Helmholtz and modified Helmholtz equations are related to various physical applications in science and engineering. More specifically, these equations are used to describe the Debye-Hückel equation [15], the scattering of a wave [17], the linearization of the Boltzmann equation [35], the vibration of a structure [6], the acoustic cavity problem [12], the radiation wave [19] and the steady-state heat conduction in fins [33]. In general, we assume the knowledge of the geometry of the domain of interest, the boundary conditions on the entire boundary of the solution domain and the so-called wave parameter, κ, and this gives rise to *direct/forward problems* for Helmholtz-type equations, which have been extensively studied both mathematically and numerically, e.g. [24, 34]. When one or more of the above conditions for solving the direct problem associated with Helmholtz-type equations are partially or entirely unknown, then an *inverse problem* may be formulated to determine the unknowns from additional responses.

Traditional numerical methods, in conjunction with an appropriately chosen regularization/stabilization method, have been employed to solve inverse problems associated with Helmholtz-type equations, such as the finite-difference method (FDM) [4, 5], the finite element method (FEM) [25, 26] and the boundary element method (BEM) [39, 40], respectively. Both the FDM and the FEM require the discretization of the domain of interest which is time consuming and tedious, especially for complicated geometries. On the other hand, while the BEM is a boundary discretization method and hence reduces the dimensionality of the problem by one, however it requires the evaluation of singular integrals involving the fundamental solution and its normal derivative and the corresponding BEM matrices are fully populated.

An alternative to these traditional numerical methods are the so-called *meshless methods* which have been used extensively in the last two decades for retrieving accurate, stable and convergent numerical solutions to inverse problems for Helmholtz-type equations. The advantages of meshless methods are the ease with which they can be implemented, in particular for problems in complex geometries, their low computational cost and the fact that, in general, they are exempted from integrations that may become cumbersome, especially in three dimensions. Such methods include the boundary particle method (BPM) [13], the singular boundary method (SBM) [14], the method of fundamental solutions (MFS) [16], the boundary knot method (BKM) [23], Kansa's method [28], etc.

The plane waves method (PWM) is a meshless Trefftz method applicable to the solution of boundary value problems governed by the Helmholtz or modified Helmholtz equation, [1, 2, 44], see also [20, Section 11.1.3]. The PWM has since been applied to the modified Helmholtz equation in [36], for the calculation of the eigenfrequencies of the Laplace operator in [3] and for the solution of inverse problems of Cauchy type in [22]. More recently, it was applied to the solution of direct axisymmetric Helmholtz problems in [29].

The PWM is closely related to another meshless Trefftz method, the method of fundamental solutions (MFS) [16] which has in recent years become very popular for the solution of inverse problems [31, 32]. The reason for this popularity is due to the fact that it is meshless and of boundary type, hence the MFS is easy to implement for problems in complex geometries in two and three dimensions. These properties are shared by the PWM which was shown to be an asymptotic version of the MFS in [2]. Moreover, the PWM has a considerable advantage over the MFS as it does not require an external pseudo-boundary on which the sources are to be placed. The location of this pseudo-boundary has been a major issue in the application of the MFS [11].

The PWM has apparently never been applied to *inverse geometric problems* [32] and in this study we investigate its application to a particular class of such inverse problems, namely *boundary identification problems*. For Helmholtz-type equations such problems have been solved using the BEM in [37] and the MFS in [7, 38]. The paper is organized as follows. In Section 2 we present the inverse geometric problem under investigation. The numerical method employed for the approximate solution of the problem, namely the PWM, and the Tikhonov regularization method are described in Section 3. Five examples are considered and thoroughly investigated in Section 4. Finally, some concluding remarks and ideas for future work are presented in Section 5.

2. The problem

We consider the inverse geometric boundary value problem given by

$$\Delta u + \kappa^2 u = 0 \quad \text{in} \quad \Omega, \tag{2.1a}$$

where $\kappa \in \mathbb{C}^*$ is given, subject to the Cauchy boundary conditions

$$u = g_1 \quad \text{and} \quad \frac{\partial u}{\partial n} = g_2 \quad \text{on} \quad \partial\Omega_1, \tag{2.1b}$$

and the Robin boundary condition

$$\alpha u + \beta \frac{\partial u}{\partial n} = g_3 \quad \text{on} \quad \partial\Omega_2, \tag{2.1c}$$

where Ω is a simply-connected bounded domain in $\mathbb{R}^2$ with smooth or piecewise smooth boundary $\partial\Omega$ partitioned into two disjoint parts $\partial\Omega_1$ (known) and $\partial\Omega_2$ (unknown), and g_1, g_2, g_3 are given functions. In (2.1b) and (2.1c), $\partial/\partial n$ is the partial derivative along the outward normal unit vector $\boldsymbol{n} = (n_x, n_y)$ to the boundary at the point (x, y), and α and β are given coefficients satisfying $\alpha\beta \geq 0$. A Dirichlet or Neumann boundary condition in (2.1c) is obtained if $\alpha = 1, \beta = 0$ or $\alpha = 0, \beta = 1$, respectively. If κ is real and positive representing the wave number, then equation (2.1a) becomes the Helmholtz equation in acoustic scattering, whilst if $\kappa = i\lambda$ with $i = \sqrt{-1}$ and λ real and positive representing a heat transfer coefficient, then equation (2.1a) becomes the modified Helmholtz equation governing heat conduction in fins.

In problem (2.1a)-(2.1c) the goal is to determine u as well as the boundary $\partial\Omega_2$. This portion of the boundary is presumed damaged due to a possible corrosion attack and the corrosion coefficient $\gamma := \beta/\alpha$ is also known as the impedance coefficient. Physically, in general we have that in (2.1c), $g_3 = 0$. Uniqueness of solution $(u, \partial\Omega_2)$ satisfying (2.1a), (2.1b) and (2.1c) holds [21] in the case of a perfectly conducting boundary ($\alpha = 1, \beta = 0, g_3 = 0$) on which

$$u = 0 \quad \text{on} \quad \partial\Omega_2, \tag{2.1d}$$

or an insulated boundary $(\alpha = 0, \beta = 1, g_3 = 0)$ on which

$$\frac{\partial u}{\partial n} = 0 \quad \text{on} \quad \partial\Omega_2, \tag{2.1e}$$

provided that $g_2 \not\equiv 0$ (or $g_1 \not\equiv$ constant). In the case of a homogeneous Robin boundary condition

$$u + \gamma \frac{\partial u}{\partial n} = 0 \quad \text{on} \quad \partial\Omega_2, \tag{2.1f}$$

there exist counterexamples, [7], for which uniqueness of solution fails.

Prior to this paper, the inverse geometric problem (2.1a)-(2.1c) has been solved using the BEM in [37] and the MFS in [38], and it is the purpose of this study to develop the PWM for solving the same problem. In addition, we make a comparison between the MFS and the PWM and also investigate a physical example with $g_3 = 0$.

3. THE PLANE WAVES METHOD

In the PWM [2], we approximate the solution u of boundary value problem (2.1a)-(2.1c) by a linear combination of plane waves

$$u_L(\boldsymbol{x}) = \sum_{\ell=1}^{L} a_\ell \mathrm{e}^{\mathrm{i}\kappa\boldsymbol{x}\cdot\boldsymbol{d}_\ell}, \qquad \boldsymbol{x} = (x, y) \in \overline{\Omega}. \tag{3.1}$$

The justification of the PWM approximation (3.1) is based on the fact that the span of the set of plane wave functions $\left\{\mathrm{e}^{\mathrm{i}\kappa\boldsymbol{x}\cdot\boldsymbol{d}} \mid \boldsymbol{d} = \left(\cos\varphi, \sin\varphi\right), \varphi \in [0, 2\pi)\right\}$ is dense, in the $L^2(\Omega)$-norm, in the set of functions satisfying equation (2.1a), [10]. In (3.1), the vectors $\boldsymbol{d}_\ell$ are unitary direction vectors with distinct directions and, clearly, each plane wave in the above expansion satisfies the Helmholtz equation (2.1a). As a result, in order to determine the unknown complex coefficients $\{a_\ell\}_{\ell=1}^{L}$ we only need to satisfy the boundary conditions of the boundary value problem in question, in our case (2.1b) and (2.1c). Density results regarding approximation (3.1) may be found in [2] where it is also shown that the PWM may be viewed as an asymptotic version of the MFS.

In the PWM we select $M + 1$ uniformly distributed boundary collocation points on $\partial\Omega_1$ and $N - 1$ uniformly distributed boundary collocation points on $\partial\Omega_2$. In particular, if the domain $\Omega = \{(r(\vartheta), \vartheta) \mid \vartheta \in [0, 2\pi)\}$ is a star-like domain, we choose the boundary points on $\partial\Omega_1$ to be, in polar coordinates,

$$\boldsymbol{x}_m = r_m \left(\cos\vartheta_m, \sin\vartheta_m\right), \quad \vartheta_m = \frac{(m-1)\pi}{M}, \quad m = 1, \ldots, M + 1, \tag{3.2}$$

while the boundary collocation points on $\partial\Omega_2$ are

$$\boldsymbol{x}_{M+1+j} = r_{M+1+j} \left(\cos\theta_j, \sin\theta_j\right), \quad \theta_j = \pi + \frac{j\pi}{N}, \quad j = 1, \ldots, N - 1, \tag{3.3}$$

where

$$r_m = r(\vartheta_m), \quad m = 1, \ldots, M + 1, \tag{3.4a}$$

and

$$r_{M+1+j} = r(\theta_j), \quad j = 1, \ldots, N - 1, \tag{3.4b}$$

Moreover, we choose the L unitary direction vectors to be

$$\boldsymbol{d}_\ell = \left(\cos\varphi_\ell, \sin\varphi_\ell\right), \quad \varphi_\ell = \frac{2(\ell-1)\pi}{L}, \quad \ell = 1, \ldots, L. \tag{3.5}$$

Clearly, there could be other choices for the L unitary direction vectors $\boldsymbol{d}_\ell$, $\ell = 1, \ldots, L$. The proposed choice given in (3.5) is the simplest such choice guaranteeing the distinct directions of these vectors and, moreover, it provides a uniform distribution of the plane waves directions in the PWM (see [2]).

3.1. **Implementational details.** In the PWM described above we have a total of $2L+N-1$ unknowns consisting of the $2L$ unknown coefficients $\boldsymbol{a} = \{a_\ell = \alpha_\ell + \mathrm{i}\beta_\ell\}_{\ell=1}^L$, as well as the $N-1$ unknown positive radii values $\boldsymbol{r} = \{r_{M+1+n}\}_{n=1}^{N-1}$. These are determined by imposing the boundary conditions (2.1b) and (2.1c). By imposing boundary conditions (2.1b) at the $M+1$ points (3.2) we obtain $4(M+1)$ equations (taking real and imaginary parts) and by imposing boundary condition (2.1c) at the $N-1$ points (3.3) we obtain a further $2(N-1)$ equations. Thus, the total number of equations is $4M+2N+2$ and for a determined or over-determined situation we therefore need to have $4M+N \geq 2L-3$. The imposition of the boundary conditions (2.1b) and (2.1c) is achieved by minimizing the regularized non-linear least-squares functional

$$
\begin{aligned}
\mathcal{F}(\boldsymbol{a}, \boldsymbol{r}) = {}& \sum_{m=1}^{M+1} \left| u_L(\boldsymbol{x}_m) - g_1(\boldsymbol{x}_m) \right|^2 + \sum_{m=1}^{M+1} \left| \frac{\partial u_L}{\partial n}(\boldsymbol{x}_m) - g_2(\boldsymbol{x}_m) \right|^2 \\
& + \sum_{j=1}^{N-1} \left| \alpha u_L(\boldsymbol{x}_{M+1+j}) + \beta \frac{\partial u_L}{\partial n}(\boldsymbol{x}_{M+1+j}) - g_3(\boldsymbol{x}_{M+1+j}) \right|^2 \\
& + \lambda_1 \sum_{\ell=1}^{L} |a_\ell|^2 + \lambda_2 \sum_{j=2}^{N-1} \left(r_{M+1+j} - r_{M+1+j-1} \right)^2,
\end{aligned}
\tag{3.6}
$$

where $\lambda_1, \lambda_2 \geq 0$ are regularization parameters and $|\cdot|$ denotes the modulus of a complex number.

Remarks.

(i) The normal derivative flux data in (2.1b) comes from practical measurement which is inherently contaminated with noisy errors, and therefore we replace g_2 by g_2^ϵ given by

$$
g_2^\epsilon(\boldsymbol{x}_m) = (1 + \rho_m p) g_2(\boldsymbol{x}_m), \quad m = \overline{1, (M+1)},
\tag{3.7}
$$

where p represents the percentage of noise and ρ_j is a pseudo-random noisy variable drawn from a uniform distribution in $[-1, 1]$ using the MATLAB$^©$ command `-1+2*rand(1,M+1)`.

(ii) In (3.6), the outward normal vector $\boldsymbol{n}$ is defined as follows:

$$
\boldsymbol{n}(\vartheta) = \frac{1}{\sqrt{r^2(\vartheta) + r'^2(\vartheta)}} \left[(r'(\vartheta)\sin\vartheta + r(\vartheta)\cos\vartheta)\,\boldsymbol{i} - (r'(\vartheta)\cos\vartheta - r(\vartheta)\sin\vartheta)\,\boldsymbol{j} \right],
\tag{3.8}
$$

where $\boldsymbol{i} = (1,0)$ and $\boldsymbol{j} = (0,1)$. In (3.8), we use the finite-difference approximation

$$
r'(\vartheta_i) \approx \frac{r_{i+1} - r_{i-1}}{2\pi/N}, \quad i = \overline{M+2, M+N},
\tag{3.9}
$$

with the convention that $r_{M+N+1} = r_1$.

(iii) The last term in (3.6) imposes a C^1-smoothness constraint on the unknown boundary $\partial\Omega_2$. In previous studies, [8, 30], we imposed a C^0-continuity constraint for similar shape detection problems, but, after extensive experimentation, found that the results with the higher-order C^1-smoothness are more accurate. Of course, to impose the correct degree of smoothness requires *a priori* knowledge about the regularity of the unknown boundary, e.g. if it is known that $\partial\Omega_2$ has corners, then a total variation constraint, [9], would be more appropriate. Finally, it should be noted that in the absence of such *a priori* information on the smoothness of the unknown boundary, one does not need to penalise it, but instead needs to stop the iteration process at an appropriate threshold. More details regarding general optimisation for nonlinear and ill-posed problems can be found in [27].

(iv) The minimization of functional (3.6) is carried out using the MATLAB$^©$ optimization toolbox routine `lsqnonlin` which solves nonlinear least squares problems. The routine `lsqnonlin` does not require the user to provide the gradient and, in addition, it offers the option of imposing lower and upper bounds on the elements of the vector of unknowns $(\boldsymbol{a}, \boldsymbol{r})$ through the vectors `lb` and `up`. In our problem, there are no

bounds on $\boldsymbol{a}$ but $\boldsymbol{r}$ is bounded between 0 and 1.2 (for Examples 1-5). Unless otherwise stated, we took the initial guess $(\boldsymbol{a}^0, \boldsymbol{r}^0) = (\boldsymbol{0}, \boldsymbol{0.5})$.

(v) In the implementation of the method, we split the unknown coefficients $\boldsymbol{a} = \{a_\ell\}_{\ell=1}^L$ into real and imaginary parts $\{a_\ell = \alpha_\ell + \mathrm{i}\beta_\ell\}_{\ell=1}^L$. In $\mathtt{lsqnonlin}$ (which can only handle real variables) all the unknowns are real and consist of the $2L$ real and imaginary parts of the coefficients $\{\alpha_\ell\}_{\ell=1}^L$ and $\{\beta_\ell\}_{\ell=1}^L$, respectively, and the radii values $\boldsymbol{r} = \{r_{M+1+n}\}_{n=1}^{N-1}$. For the imposition of the boundary conditions (2.1b) and (2.1c), the complex approximation (3.1) is obtained from first constructing the complex coefficients $\{a_\ell\}_{\ell=1}^L$ from their real and imaginary parts. The boundary conditions (2.1b) and (2.1c) are imposed by imposing the satisfaction of both their real and the imaginary parts. Thus the functions provided to $\mathtt{lsqnonlin}$ are all real.

4. NUMERICAL EXAMPLES

In all figures presented in this section the reconstructed boundary is shown in red dots ($\cdots$). In numerical Examples 1 and 2 below we chose $\kappa = \sqrt{2}$ and consider boundary data g_1, g_2 and g_3 constructed from the analytical solution

$$u(x,y) = \mathrm{e}^{ax+by}, \tag{4.1}$$

where $a = 0.1$ and $b = \mathrm{i}\sqrt{a^2 + \kappa^2}$.

4.1. **Example 1.** We first consider the unit disk Ω in which $\partial\Omega_1$ and $\partial\Omega_2$ are the upper and lower semicircle, respectively, that is,

$$\partial\Omega_1 = \left\{\boldsymbol{x} = (x,y)| -1 \le x \le 1; y = \sqrt{1-x^2}\right\} \tag{4.2a}$$

and

$$\partial\Omega_2 = \left\{\boldsymbol{x} = (x,y)| -1 \le x \le 1; y = -\sqrt{1-x^2}\right\}. \tag{4.2b}$$

4.2. **Example 2.** We next consider a peanut-shaped domain described parametrically by

$$\Omega = \left\{\boldsymbol{x} = (x,y)|x^2 + y^2 < r^2(\vartheta); \ \vartheta \in [0, 2\pi)\right\}, \quad \text{where} \quad r(\vartheta) = \sqrt{\cos^2\vartheta + \frac{1}{4}\sin^2\vartheta} \tag{4.3}$$

and $\partial\Omega_1$ and $\partial\Omega_2$ are defined by

$$\partial\Omega_1 = \{\boldsymbol{x} = (x,y)|x = r(\vartheta)\cos\vartheta; y = r(\vartheta)\sin\vartheta, \ \vartheta \in [0,\pi]\}, \tag{4.4a}$$

$$\partial\Omega_2 = \{\boldsymbol{x} = (x,y)|x = r(\vartheta)\cos\vartheta; y = r(\vartheta)\sin\vartheta, \ \vartheta \in (\pi, 2\pi)\}. \tag{4.4b}$$

In Figures 1 and 3 we present some results with no noise and no regularization for $\alpha = 1, \beta = 0$ (Dirichlet boundary condition on $\partial\Omega_2$) and $M = 10, N = 20, L = 20$ for various numbers of iterations, for Examples 1 and 2, respectively. The corresponding results for $\alpha = 0, \beta = 1$ (Neumann boundary condition on $\partial\Omega_2$) are presented in Figures 2 and 4. From Figures 1-4 it can be seen that in case of no noise the iterative reconstructions are convergent to the true shapes (4.2b) and (4.4b) for both Examples 1 and 2, respectively, and for both Dirichlet and Neumann problems in about 2000 iterations. It can be observed that for the Neumann problem convergence is reached after about 1000 iterations whilst for the Dirichlet problem convergence requires more iterations, i.e., the iterative method converges faster for the former problem than for the latter problem. An argument regarding the number of iterations will be presented in the next paragraph.

Next, we introduce $p = 10\%$ noise, as described in equation (3.7). We only illustrate the reconstructions for Example 2, as similar results have been obtained for Example 1. Similarly, for brevity, we only illustrate the numerical results for the Neumann problem with $\alpha = 0, \beta = 1$. The results obtained without and with regularization in either λ_1 or λ_2 are presented in Figures 5-7. First, from Figure 5 it can be seen that in the case of no regularization, i.e., $\lambda_1 = \lambda_2 = 0$, the numerical reconstructions after 1000 to 2000 iterations are reasonable but with some slight

oscillations manifesting, especially near the points where the boundaries $\partial\Omega_1$ and $\partial\Omega_2$ meet. These oscillations are likely to grow, as the number of iterations increases, due to the instability of the nonlinear ill-posed problem. In order to restore stability, regularization is employed. As stability is ensured through appropriate choices of the regularization parameters λ_1 and/or λ_2, there is no need to cease the iteration process at a threshold dictated by a discrepancy-type stopping criterion. In this situation, the iterative process can be allowed to run until no further progress is realised and convergence has achieved a level of stationarity (in our case, in around 2000 iterations). The numerical reconstructions after 2000 iterations presented in Figures 6 and 7 show that regularization with λ_1 retrieves very accurately the desired shape (4.4b) whilst regularization with λ_2 has less of an effect. From Figure 7 one would probably choose a regularization parameter λ_2 between 10^{-2} and 10^{-1}, but from Figure 6 one can see that a wide range of values of λ_1 between 10^{-10} and 10^{-4} all produce stable and very accurate results.

4.3. **Example 3.** We investigate an example considered in [38] given by $\kappa = 1$ and

$$u(x,y) = \cos\left(\frac{x+y}{\sqrt{2}}\right) \tag{4.5}$$

in the unit circle with $\partial\Omega_1$ and $\partial\Omega_2$ given by (4.2a) and (4.2b), respectively. We consider the Neumann case $\alpha = 0, \beta = 1$. We took $M = 12, N = 12, L = 14$ with initial guess $(\boldsymbol{a}^0, \boldsymbol{r}^0) = (\boldsymbol{0}, \boldsymbol{0.55})$ and examined the effect of regularization with noise $p = 5\%$. Similar results have been obtained for $p = 10\%$ and are therefore not presented. The effects of regularization with λ_1 or λ_2, after 2000 iterations, are presented in Figures 8 and 9, respectively. From these figures, it can be seen that regularization with λ_1 between 10^{-5} and 10^{-3}, or with λ_2 between 10^{-3} and 10^1 produces stable and accurate reconstructions of the semicircular shape (4.2b). In order to give a justification for the choice of the regularization parameters, the L-curves, see [18], are plotted in Figure 10. From this figure, it can be seen that L-shaped curves are indeed obtained when plotting, on a log-log scale, the residual (given by the square root of the first three terms in the right-hand side of (3.6)) versus the solution norm $||\boldsymbol{a}||$ or $||\boldsymbol{r}'||$ given by the square root of the fourth or fifth term, respectively, in the right-hand side of (3.6). Then, selecting values of λ_1 or λ_2 near the corners of these L-curves provide suitable candidates for appropriate regularization parameters, balancing smoothing versus stability.

We finally mention that the results obtained with the PWM in Figures 8 and 9 are comparable to those in Figure 10(b) in [38] which were obtained using the MFS, parametrization of $\partial\Omega_2$ by a function $y = f(x)$ with regularization using the NAG [42] Fortran routine E04UNF from the initial guess $y = 0$ for $-1 < x < 1$. This is to be expected since the PWM may be viewed as an asymptotic version of the MFS as the source points move further away from the simply connected bounded domain Ω, [2]. The PWM is also faster than the MFS because, in two-dimensions, the plane waves are calculated faster than Bessel functions.

4.4. **Example 4.** We next consider a physical example (with $g_3 = 0$) given by the homogeneous Robin boundary condition (2.1f) with the corrosion coefficient

$$\gamma(\vartheta) = \frac{1}{-\tau\sin(\vartheta) + \frac{\pi}{4}\cos(\vartheta)\tan\left(\frac{\pi}{4}\cos(\vartheta)\right)}, \tag{4.6}$$

where $\tau = \sqrt{\frac{\pi^2}{16} - \kappa^2}$ and we take $\kappa = 1/\sqrt{2}$. We take $\partial\Omega_1$ and $\partial\Omega_2$ given by (4.2a) and (4.2b), respectively, and then one may easily verify that $\gamma(\vartheta) > 0$ for $\vartheta \in [\pi, 2\pi)$, i.e. $\gamma > 0$ on $\partial\Omega_2$. The analytical solution is taken as

$$u(x,y) = \sqrt{2}\,\mathrm{e}^{\tau y}\cos\left(\frac{\pi x}{4}\right), \tag{4.7}$$

from which the Cauchy data (2.1b) on $\partial\Omega_1$ is constructed. We took $M = 16, N = 16, L = 20$ and initial guess $(\boldsymbol{a}^0, \boldsymbol{r}^0) = (\boldsymbol{0}, \boldsymbol{0.55})$. In Figure 11 we present some results with no noise and no regularization for various numbers of iterations. From this figure, it can be seen that convergence to the exact shape (4.2b) is achieved within 1000 iterations. The effects of regularization with λ_1 keeping $\lambda_2 = 0$, and λ_2 keeping $\lambda_1 = 0$, for noise $p = 7\%$ and 8000

iterations are presented in Figures 12 and 13, respectively. From these figures, it can be seen that regularization with λ_1 between 10^{-10} and 10^{-9} or with λ_2 between 10^{-1} and 10^0 produces stable and accurate reconstructions of the semicircular shape (4.2b).

4.5. **Example 5.** We finally consider a square of side $\sqrt{2}$ rotated by $\pi/4$ with boundaries $\partial\Omega_1$ and $\partial\Omega_2$ defined by

$$\partial\Omega_1 = \{\boldsymbol{x} = (x,y)|0 \le x \le 1; y = 1 - x\} \cup \{\boldsymbol{x} = (x,y)|-1 \le x \le 0; y = 1 + x\}, \tag{4.8a}$$

$$\partial\Omega_2 = \{\boldsymbol{x} = (x,y)|-1 \le x \le 0; y = -1 - x\} \cup \{\boldsymbol{x} = (x,y)|0 \le x \le 1; y = -1 + x\}. \tag{4.8b}$$

We considered the Neumann case $\alpha = 0, \beta = 1$ and took the exact solution (4.1) with $a = 1$, $b = \mathrm{i}\sqrt{a^2 + \kappa^2}$ and $\kappa = \sqrt{2}$. The initial guess was $(\boldsymbol{a}^0, \boldsymbol{r}^0) = (\mathbf{0}, \mathbf{0.65})$ and $M = 21, N = 21, L = 20$. The effects of regularization with λ_1 or λ_2, after 2000 iterations, for $p = 10\%$ noise are presented in Figures 14 and 15, respectively. From these figures, it can be seen that stable and accurate reconstructions of the right-angle wedge shape (4.8b) are obtained.

5. Conclusions

In this work, the PWM was successfully applied, apparently for the first time, for obtaining stable and accurate solutions of an inverse problem associated with two-dimensional Helmholtz-type equations, namely the reconstruction of an unknown portion of the boundary from a given exact boundary condition on this part of the boundary and additional noisy Cauchy data on the remaining known portion of the boundary. This inverse geometric problem is ill-posed and in discrete form yields an ill-conditioned system of nonlinear equations, which was solved, in a stable manner, by employing the Tikhonov regularization method [43]. The value of the regularization parameter was chosen according to Hansen's L-curve criterion [18]. Five examples for two-dimensional simply connected, convex and non-convex domains and having smooth and piecewise smooth boundaries, were considered. From the numerical experiments, it can be concluded that the proposed method is stable with respect to noise in the Cauchy data. Furthermore, it is accurate and computationally very efficient. The application of the PWM for the detection of internal defects as well as to three-dimensional inverse geometric problems will be the subject of future research.

References

[1] C. J. S. Alves and S. S. Valtchev, *Numerical simulation of acoustic wave scattering using a meshfree plane waves method*, International Workshop on Meshfree Methods, 2003, `http://www.math.ist.utl.pt/meshfree/silen.pdf`.

[2] C. J. S. Alves and S. S. Valtchev, *Numerical comparison of two meshfree methods for acoustic wave scattering*, Eng. Anal. Bound. Elem. **29** (2005), 371–382.

[3] P. R. S. Antunes, *Numerical calculation of eigensolutions of 3D shapes using the method of fundamental solutions*, Numer. Methods Partial Differential Equations **27** (2011), 1525–1550.

[4] F. Berntsson, V. A. Kozlov, L. Mpinganzima and B. O. Turesson, *An alternating iterative procedure for the Cauchy problem for the Helmholtz equation*, Inverse Problems Sci. Eng. **22** (2014), 45–62.

[5] F. Berntsson, V. A. Kozlov, L. Mpinganzima and B. O. Turesson, *An accelerating alternating iterative procedure for the Cauchy problem for the Helmholtz equation*, Comput. Math. Appl. **68** (2014), 44–60.

[6] D. E. Beskos, *Boundary element method in dynamic analysis: Part II (1986–1996)*, ASME Appl. Mech. Rev. **50** (1997), 149–197.

[7] B. Bin-Mohsin and D. Lesnic, *Identification of a corroded boundary and its Robin coefficient*, East Asian J. Appl. Math. **2** (2012), 126–149.

[8] D. Borman, D. B. Ingham, B. T. Johansson and D. Lesnic, *The method of fundamental solutions for detection of cavities in EIT*, J. Integral Equations Appl. **21** (2009), 381–404.

[9] A. Borsic, B. M. Graham, A. Adler and W.R.B. Lionheart, *In vivo impedance imaging with total variation regularization*, IEEE Trans. Med. Inaging **29** (2010), 44–54.

[10] O. Cessenat and B. Després, *Using plane waves as base functions for solving time harmonic equations with the ultra weak variational formulation*, J. Comput. Acoustics **11** (2003), 227–238.

[11] C. S. Chen, A. Karageorghis and Y. Li, *On choosing the location of the sources in the MFS*, Numer. Algor. **72** (2016), 107–130.

[12] J. T. Chen and F. C. Wong, *Dual formulation of multiple reciprocity method for the acoustic mode of a cavity with a thin partition*, J. Sound Vibration **217** (1998), 75–95.

[13] W. Chen, *Meshfree boundary particle method applied to Helmholtz problems*, Eng. Anal. Bound. Elem. **26** (2002), 577–581.

[14] W. Chen, Z. J. Fu and X. Wei, *Potential problems by singular boundary method satisfying moment condition*, CMES – Comput. Model. Eng. Sci. **54** (2009), 65–85.

[15] P. Debye and E. Hückel, *The theory of electrolytes. I. Lowering of freezing point and related phenomena*, Phys. Z. **24** (1923), 185–206.

[16] G. Fairweather and A. Karageorghis, *The method of fundamental solutions for elliptic boundary value problems*, Adv. Comput. Math. **9** (1998), 69–95.

[17] W. S. Hall and X. Q. Mao, *A boundary element investigation of irregular frequencies in electromagnetic scattering*, Eng. Anal. Bound. Elem. **16** (1995), 245–252.

[18] P. C. Hansen, *Rank-Deficient and Discrete Ill-Posed Problems: Numerical Aspects of Numerical Inversion*, SIAM, Philadelphia, 1998.

[19] I. Harari, P. E. Barbone, M. Slavutin and R. Shalom, *Boundary infinite elements for the Helmholtz equation in exterior domains*, Int. J. Numer. Meth. Eng. **41** (1998), 1105–1131.

[20] I. Herrera, *Boundary Methods: An Algebraic Theory*, Applicable Mathematics Series, Pitman (Advanced Publishing Program), Boston, MA, 1984.

[21] V. Isakov, *Inverse obstacle problems*, Inverse Problems **25** (2009), 123002 (18 pp).

[22] B. Jin and L. Marin, *The plane wave method for inverse problems associated with Helmholtz-type equations*, Eng. Anal. Bound. Elem. **32** (2008), 223–240.

[23] B. Jin and Z. Zheng, *Boundary knot method for some inverse problems associated with the Helmholtz equation*, Int. J. Numer. Meth. Eng. **62** (2005), 1636–1651.

[24] D. S. Jones, *Methods in Electromagnetic Wave Propagation*, Oxford University Press, New York, 1979.

[25] S. I. Kabanikhin and M. A. Shishlenin, *Stability analysis of a continuation problem for the Helmholtz equation*, Bull. Novosibirsk Comp. Center **16** (2013), 59–63.

[26] S. I. Kabanikhin, Y. S. Gasimov, D. B. Nurseitsov, M. A. Shishlenin, B. B. Sholpanbaev and S. Kasenov, *Regularization of the continuation problem for elliptic equations*, J. Inverse Ill-Posed Problems **21** (2013), 871–884.

[27] B. Kaltenbacher, A. Neubauer and O. Scherzer, *Iterative Regularization Methods for Nonlinear Problems*, de Gruyter, Berlin, 2008.

[28] E. J. Kansa, *Multiquadrics: A scattered data approximation scheme with applications to computational fluid dynamics*, Comput. Math Appl. **19** (1990), 147–161.

[29] A. Karageorghis, *The plane waves method for axisymmetric Helmholtz problems*, Eng. Anal. Bound. Elem. **69** (2016), 46–56.

[30] A. Karageorghis and D. Lesnic, *The method of fundamental solutions for the inverse conductivity problem*, Inverse Problems Sci. Eng. **18** (2010), 567–583.

[31] A. Karageorghis, D. Lesnic and L. Marin, *A survey of applications of the MFS to inverse problems*, Inverse Problems Sci. Eng. **19** (2011), 309–336.

[32] A. Karageorghis, D. Lesnic, and L. Marin, *The MFS for inverse geometric problems*, Inverse Problems and Computational Mechanics (L. Munteanu L. Marin and V. Chiroiu, eds.), vol. 1, Editura Academiei, Bucharest, 2011, pp. 191–216.

[33] A. D. Kraus, A. Aziz and J. Welty, *Extended Surface Heat Transfer*, John Wiley & Sons, New York, 2001.

[34] P. D. Lax and R. S. Phillips, *Scattering Theory*, Academic Press, New York, 1967.

[35] J. Lian and S. Subramanian, *Computation of molecular electrostatics with boundary element methods*, Biophys. J. **73** (1997), 1830–1841.

[36] X. Li, *On solving boundary value problems of modified Helmholtz equations by plane wave functions*, J. Comput. Appl. Math. **195** (2006), 66–82.

[37] L. Marin, *Numerical boundary identification for Helmholtz-type equations*, Comput. Mech. **39** (2006), 25–40.

[38] L. Marin and A. Karageorghis, *Regularized MFS-based boundary identification in two-dimensional Helmholtz-type equations*, CMC Comput. Mater. Continua **10** (2009), 259–293.

[39] L. Marin, L. Elliott, P. J. Heggs, D. B. Ingham, D. Lesnic and X. Wen, *Conjugate gradient-boundary element solution to the Cauchy problem for Helmholtz-type equations*, Comput. Mech. **31** (2003), 367–377.

[40] L. Marin, L. Elliott, P. J. Heggs, D. B. Ingham, D. Lesnic and X. Wen, *BEM solution for the Cauchy problem associated with Helmholtz-type equations by the Landweber method*, Eng. Anal. Bound. Elem. **28** (2004), 1025–1034.

[41] The MathWorks, Inc., 3 Apple Hill Dr., Natick, MA, *Matlab*.

[42] Numerical Algorithms Group Library Mark 21 (2007), NAG (UK) Ltd, Wilkinson House, Jordan Hill Road, Oxford, UK.

[43] A. N. Tikhonov and V. Y. Arsenin, *Methods for Solving Ill-Posed Problems*, Nauka, Moscow, 1986.

[44] S. S. Valtchev, *Numerical Analysis of Methods with Fundamental Solutions for Acoustic and Elastic Wave Propagation Problems*, Ph.D. thesis, Department of Mathematics, Instituto Superior Téchnico, Universidade Técnica de Lisboa, Lisbon, 2008.
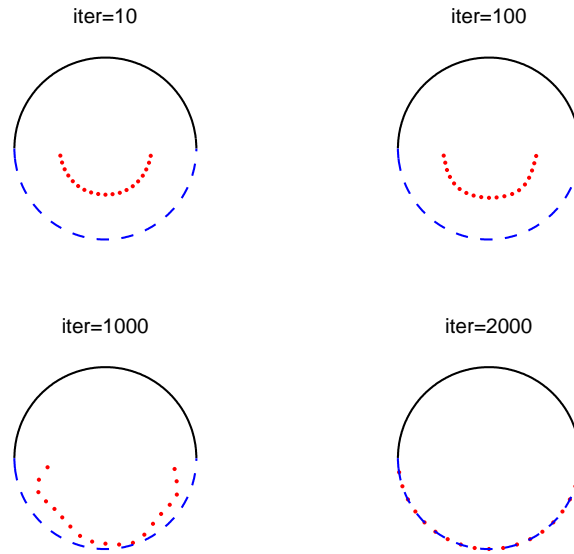
FIGURE 1. Example 1: Results for $\alpha = 1, \beta = 0$ and no noise. The reconstructed boundary is shown in red dots ($\cdots$).
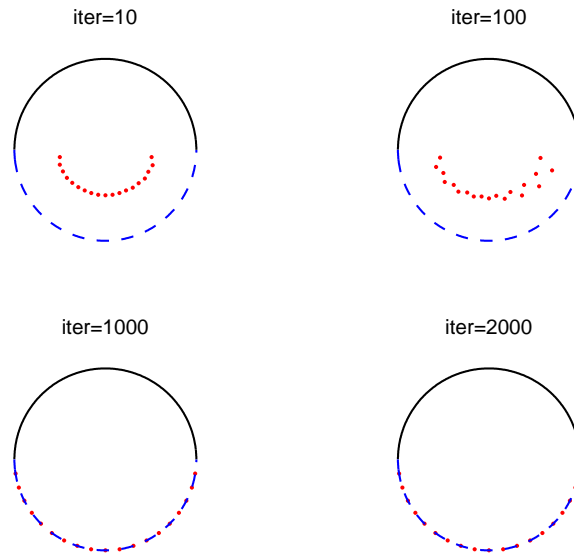

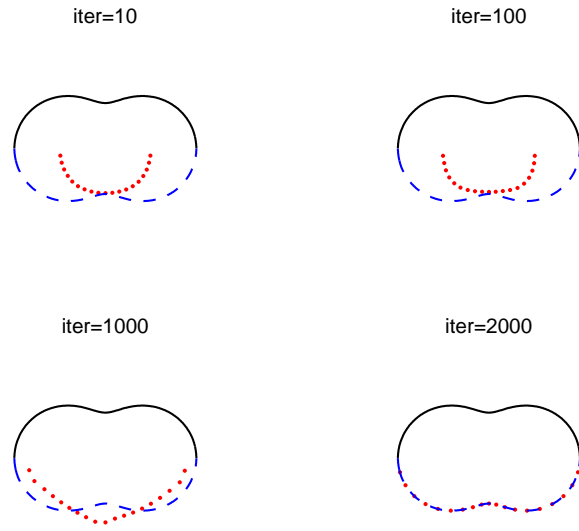FIGURE 2. Example 1: Results for $\alpha = 0, \beta = 1$ and no noise.

iter=10 iter=100

iter=1000 iter=2000

FIGURE 3. Example 2: Results for $\alpha = 1, \beta = 0$ and no noise.

iter=10 iter=100

iter=1000 iter=2000
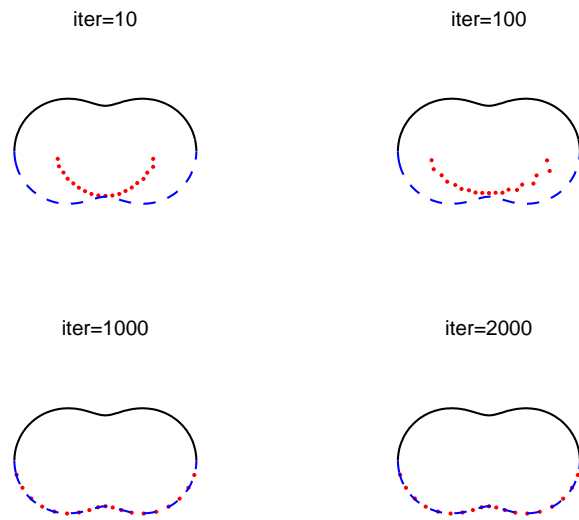
FIGURE 4. Example 2: Results for $\alpha = 0, \beta = 1$ and no noise.
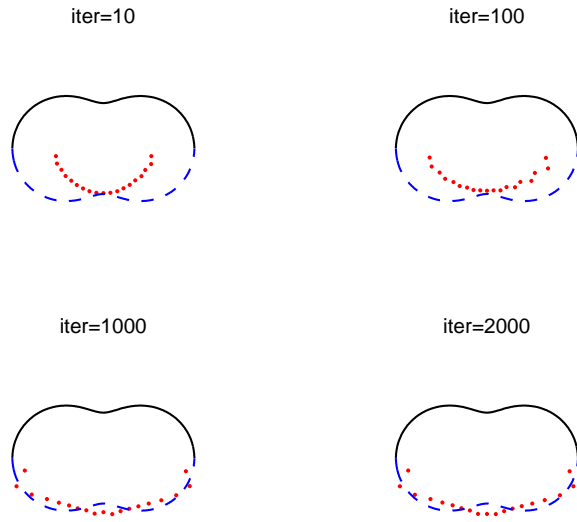
FIGURE 5. Example 2: Results for $\alpha = 0, \beta = 1$, noise $p = 10\%$ and no regularization.
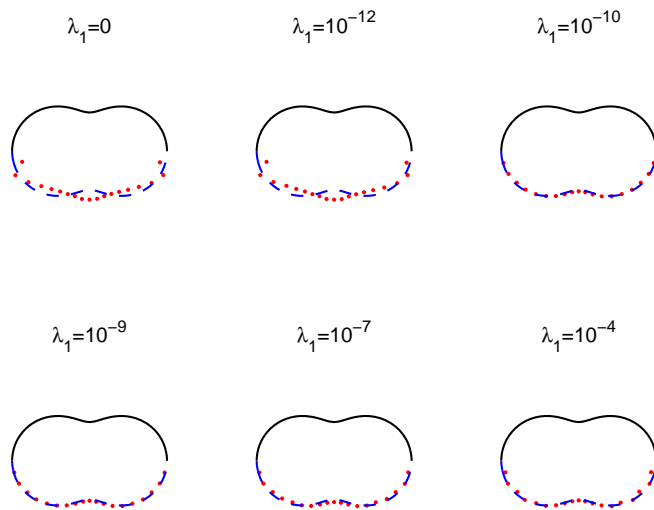
FIGURE 6. Example 2: Results for $\alpha = 0, \beta = 1$, noise $p = 10\%$, $\lambda_2 = 0$ and regularization with λ_1.
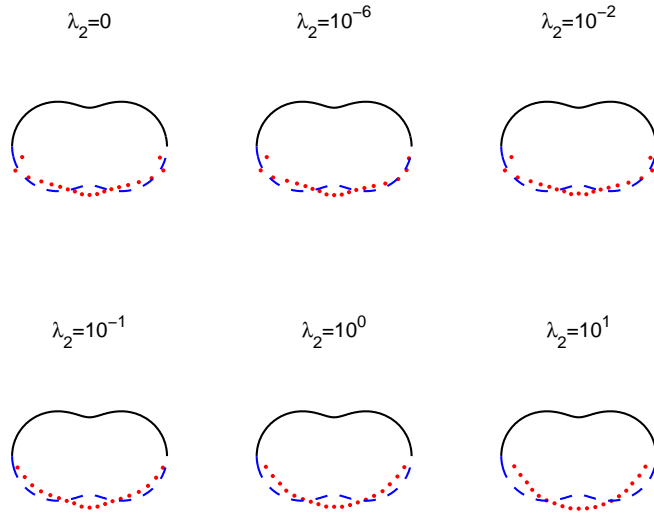
FIGURE 7. Example 2: Results for $\alpha = 0, \beta = 1$, noise $p = 10\%$, $\lambda_1 = 0$ and regularization with λ_2.
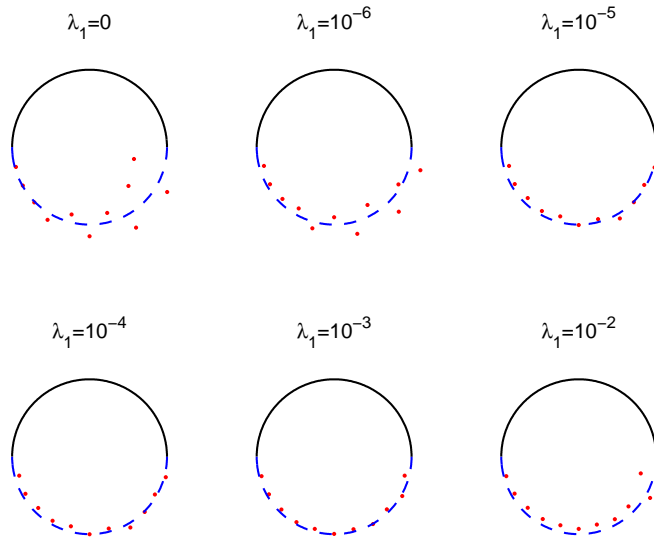
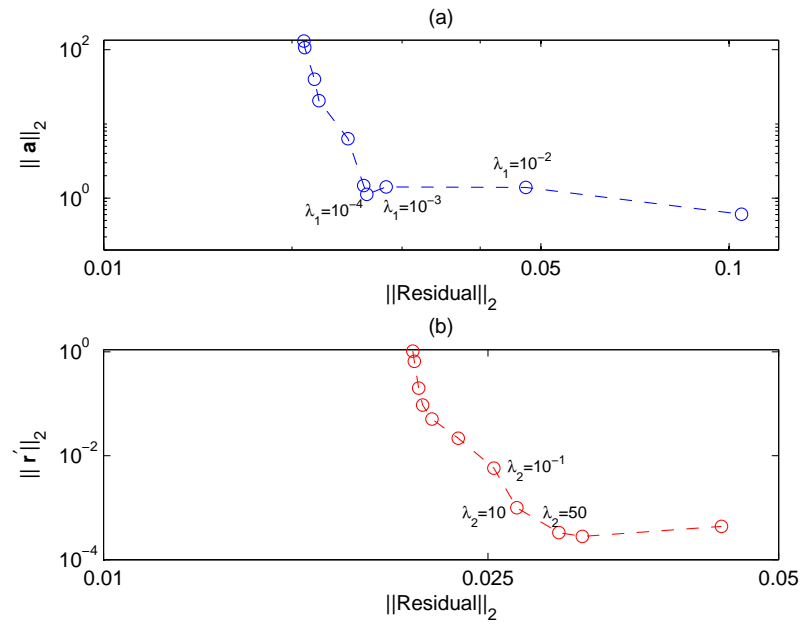FIGURE 8. Example 3: Results for noise $p = 5\%$, $\lambda_2 = 0$ and regularization with λ_1.
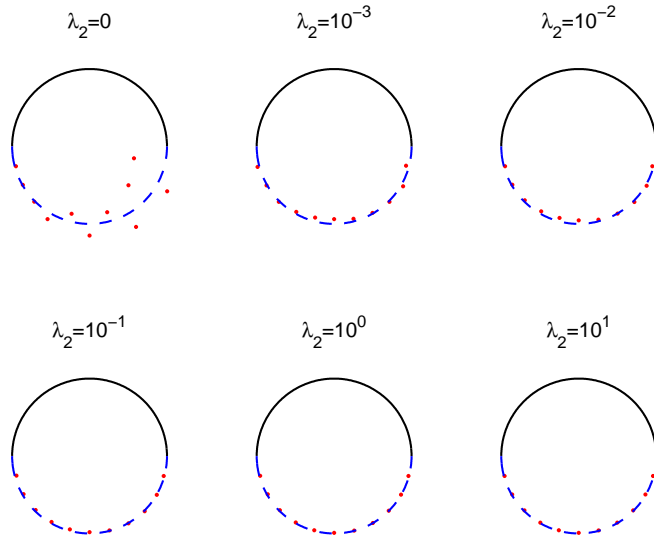
FIGURE 9. Example 3: Results for noise $p = 5\%$, $\lambda_1 = 0$ and regularization with λ_2.

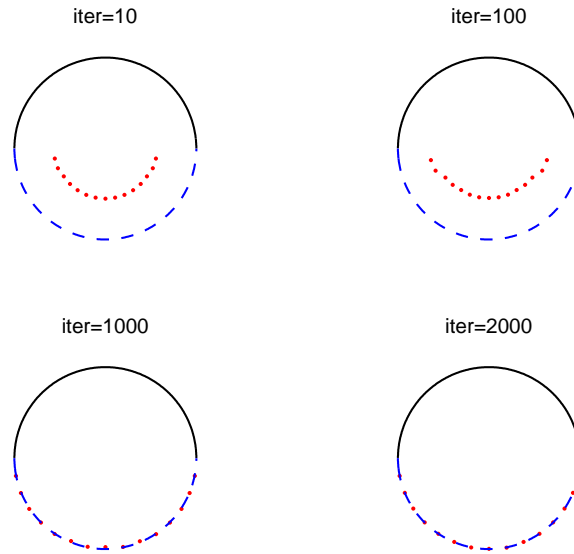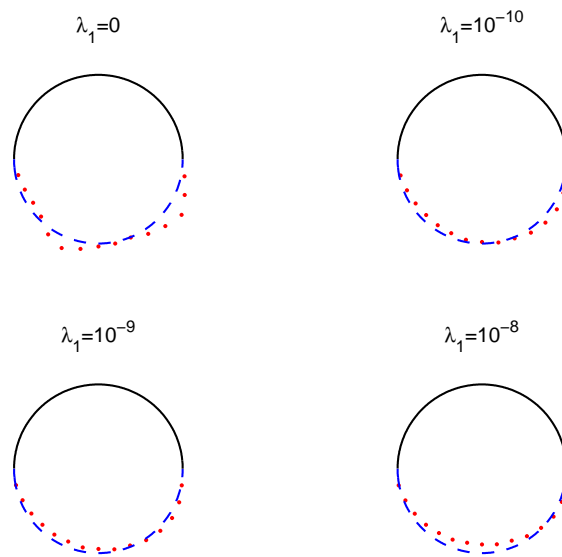FIGURE 10. Example 3: L-curves for noise $p = 5\%$. (a) Varying λ_1 while $\lambda_2 = 0$; (a) Varying λ_2 while $\lambda_1 = 0$.

iter=10   iter=100

iter=1000   iter=2000

FIGURE 11. Example 4: Results for no noise.

$\lambda_1=0$ $\lambda_1=10^{-10}$

$\lambda_1=10^{-9}$ $\lambda_1=10^{-8}$

FIGURE 12. Example 4: Results for noise $p = 7\%$, $\lambda_2 = 0$ and regularization with λ_1.
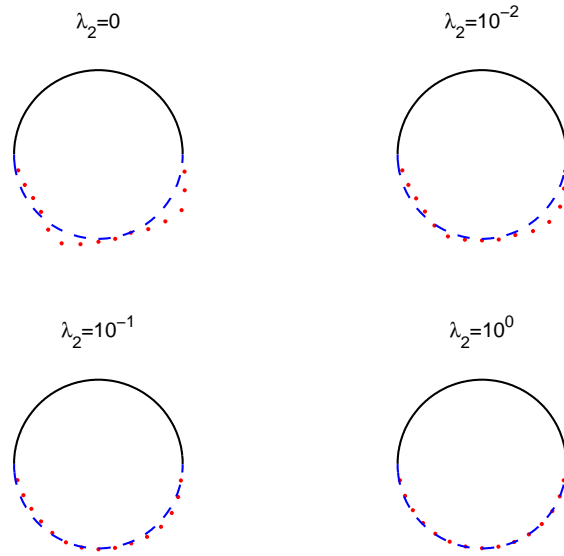
FIGURE 13. Example 4: Results for noise $p = 7\%$, $\lambda_1 = 0$ and regularization with λ_2.
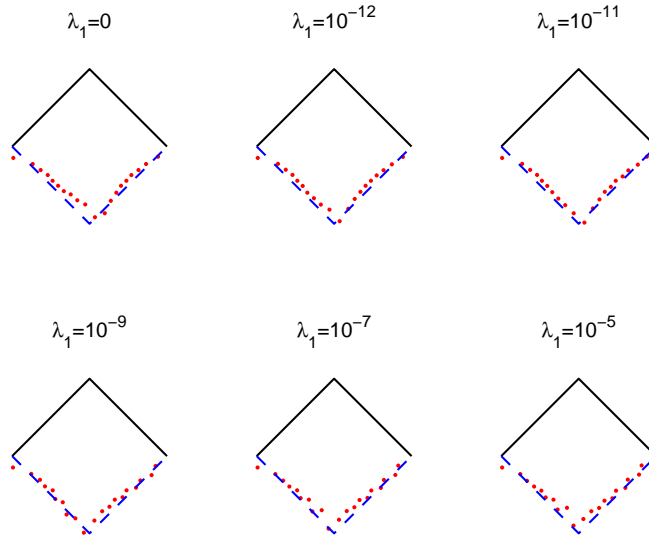
FIGURE 14. Example 5: Results for noise $p = 10\%$, $\lambda_2 = 0$ and regularization with λ_1.

DEPARTMENT OF MATHEMATICS AND STATISTICS, UNIVERSITY OF CYPRUS/ ΠΑΝΕΠΙΣΤΗΜΙΟ ΚΥΠΡΟΥ, P.O. Box 20537, NICOSIA/ΛΕΥΚΩΣΙΑ, CYPRUS/ΚΥΠΡΟΣ
E-mail address: `andreask@ucy.ac.cy`

DEPARTMENT OF APPLIED MATHEMATICS, UNIVERSITY OF LEEDS, LEEDS LS2 9JT, UK
E-mail address: `amt5ld@maths.leeds.ac.uk`

DEPARTMENT OF MATHEMATICS, FACULTY OF MATHEMATICS AND COMPUTER SCIENCE, UNIVERSITY OF BUCHAREST, 14 ACADEMIEI, 010014 BUCHAREST, AND INSTITUTE OF MATHEMATICAL STATISTICS AND APPLIED MATHEMATICS, ROMANIAN ACADEMY, 13 CALEA 13 SEPTEMBRIE, 050711 BUCHAREST, ROMANIA
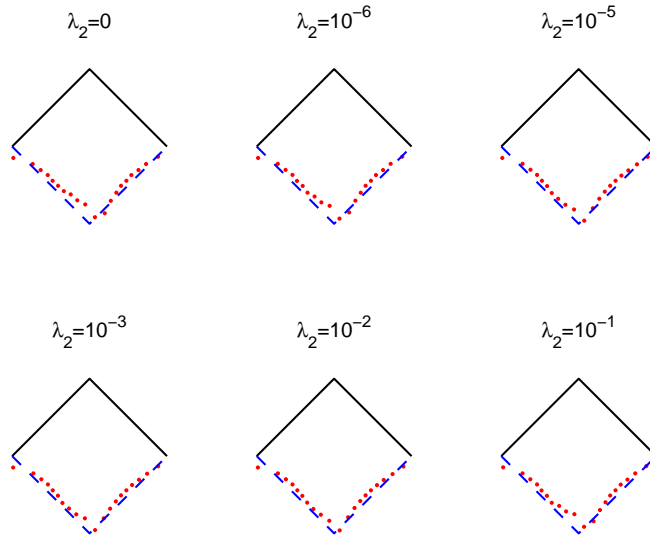*E-mail address*: `marin.liviu@gmail.com; liviu.marin@fmi.unibuc.ro`

FIGURE 15. Example 5: Results for noise $p = 10\%$, $\lambda_1 = 0$ and regularization with λ_2.